THE JOURNAL OF PHYSICAL CHEMISTRY C

Article

Cite This: J. Phys. Chem. C 2018, 122, 5657−5663

pubs.acs.org/JPCC

Plasmonic Heating Plays a Dominant Role in the Plasmon-Induced Photocatalytic Reduction of 4-Nitrobenzenethiol

Alexander A. Golubev,[†] Boris N. Khlebtsov,[†] Raul D. Rodriguez,[‡,§,*] Ying Chen,[∥] and Dietrich R. T. Zahn[‡]

[†]Institute of Biochemistry and Physiology of Plants and Microorganisms, Russian Academy of Sciences, 13 Prospekt Entuziastov, Saratov 410049, Russia

[‡]Semiconductor Physics and [∥]Institut fur Chemie, Chemnitz University of Technology, D-09107 Chemnitz, Germany

[§]Tomsk Polytechnic University, 30 Lenin Avenue, 634050 Tomsk, Russia

ABSTRACT: It is believed that plasmon-excited electrons from Ag and Au nanostructures can induce photochemical reactions. However, the influence of heat generated by nanoparticle (NP) hotspots during light irradiation was not systematically studied yet. To evaluate the role of plasmonic heating, we performed a surface-enhanced Raman spectroscopy study of the photocatalytic conversion of 4-nitrobenzenthiol to 4-aminobenzenthiol by metal NPs with different compositions and shapes having localized surface plasmon resonances (LSPRs) spanning the whole visible range. Our collective results based on temperature-dependent studies and multiwavelength analyses show that contrary to the previous reports, the photocatalytic reaction is not only determined by the excitation of LSPRs or by the NP material (Ag or Au) but also drastically dependent on the plasmon-induced heating. This work has strong implications for the development and engineering of novel plasmonic and photonic applications where the role of localized temperature must be considered.

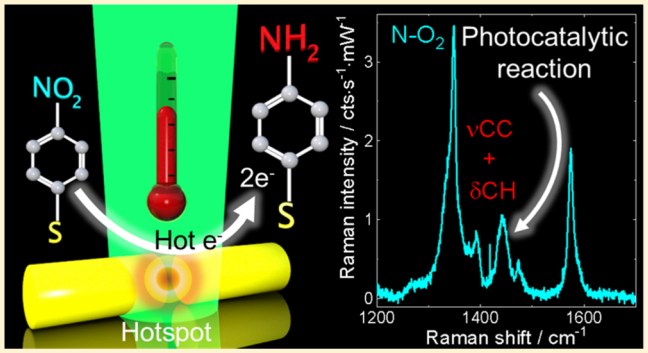

INTRODUCTION

It is well-known that the use of laser excitation in Raman spectroscopy can induce photocatalytic reactions of organic substances.[1−3] In some cases, additional catalysts such as noble metal nanoparticles (NPs) are needed to promote chemical reactions during irradiation.[4−6] NPs of noble metals show extinction in the optical region because of the unique feature known as localized surface plasmon resonance (LSPR). The strong electric field enhancement induced by NPs LSPR gives rise to an extremely high sensitivity that can allow single-molecule detection.[7] This remarkable sensitivity is now widely used in various fields to create new analytical methods in the field of surface chemistry.[8−10] The strong enhancement of local electric fields with the generation of hot electrons produced by plasmons can activate chemical reactions of organic molecules adsorbed on metal NPs.[11] The combined effects of hot electron driven plasmonic reactions have been used for liquid-phase water splitting,[12,13] hydrogen production[14] and dissociation,[15] photovoltaics,[16] and hydrocarbon conversion.[17] With such photocatalytic reactions, the molecules change their structure and the surface-enhanced Raman spectroscopy (SERS) can detect this structural change. The conversion of 4-nitrobenzenthiol (4-NBT) to 4-aminobenzenthiol (4-ABT) and *p*,*p*′-dimercaptoazobenzene on plasmonic NPs under laser irradiation[18−20] is a widely studied example of this kind of reaction partly because of their technological importance as chemical precursors for pharmaceutical drugs such as paracetamol and the easiness to obtain the self-assembly monolayer covering on plasmonic nanostructures. Most SERS platforms inducing photochemical reactions fall into three categories: (1) individual or aggregated metal NPs such as Ag,[3,8] Au,[19,20] and Cu;[21] (2) rough metal films;[22−24] and (3) gaps between metal surfaces and NPs.[18] The plasmon-induced photocatalysis depends on many experimental parameters including the plasmonic NP size, chemistry, shape, illumination power, and even time.[25] Chadha and co-workers[26] investigated the plasmon-induced oxidation and isomerization of 3-hydroxy anthranilic acid to find out whether these reactions are affected by experimental parameters such as thermal and photon energy, pH, and media such as air, nitrogen, and oxygen atmospheres. They report the SERS results obtained for a NP system measured at different temperatures that induced changes in the spectra. We aim at taking this research forward by systematically investigating how critical the localized temperature contribution is in the plasmon photocatalysis.

Despite the recent progress in the photocatalysis, the conditions necessary for the conversion of 4-NBT to 4-ABT are still under debate.[27] It was reported that this reaction could

Received: December 8, 2017
Revised: February 15, 2018
Published: February 15, 2018

DOI: 10.1021/acs.jpcc.7b12101
J. Phys. Chem. C 2018, 122, 5657−5663

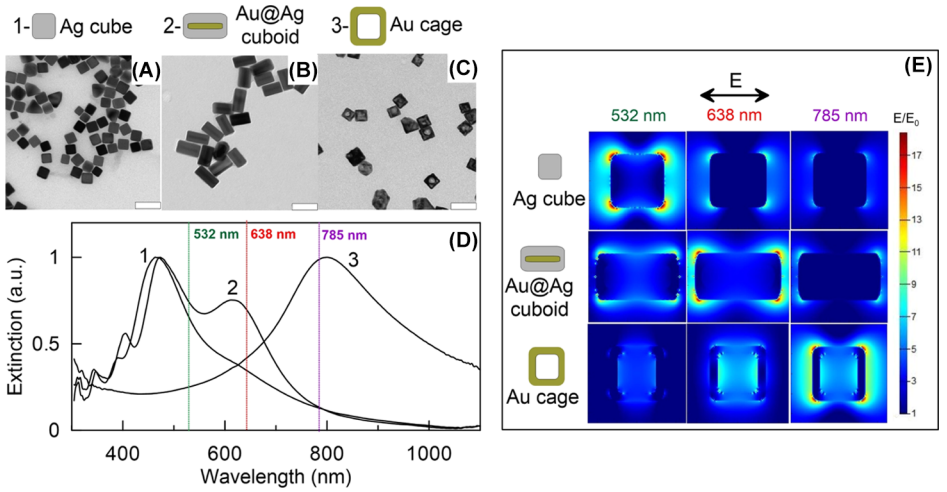

Figure 1. TEM images of as-prepared Ag nanocubes (A), Au@Ag cuboids (B), and nanocages (C). The scale bar is 100 nm for all images. Panel (D) shows the normalized extinction spectra of NPs: Ag cubes (curve 1), Au@Ag cuboids (curve 2), and nanocages (curve 3). Panel (E) shows the results of FDTD simulation of EM field distribution near the same NPs under irradiation with 514.7 nm (left), 633 nm (center), and 785 nm (right).

occur even without LSPR conditions. For example, 4-NBT molecules can be photocatalytically reduced on Ag and Cu foils under irradiation by red and green lasers.[5,21] The comparison of silver with copper and gold substrates showed that the photoreduction occurred only in the presence of silver and copper but not gold.[23] The physical mechanisms behind this reaction were believed to depend on the atomic scale catalytic active sites of metal, excitation wavelength, material (Ag vs Au), LSPR energy, hotspots, and substrate−molecule distance.[23] Moreover, the dependence of catalytic behavior on the laser power and the irradiation time was discussed in previous papers.[21,28,29] Surprisingly, although the clear consequence of increasing laser power or irradiation time was considered, the direct contribution of local temperature increase to this reaction was never discussed until now. In this context, we are interested in finding out the role of temperature increase induced in hotspots and to determine whether or not this contribution plays an essential role in the photocatalytic conversion of 4-NBT to 4-ABT used here as a model system. To this aim, we investigated SERS active photocatalysts as several NP sets with different compositions and shapes (Ag cubes, Au@Ag cuboids, and Au nanocages) having LSPRs and hotspots that can be excited under different laser wavelengths. The temperature-dependent Raman investigations on these systems as well as on 4-NBT deposited on Si and flat Ag surfaces allowed us to distinguish the photothermal plasmonic contribution from the chemical one under laser illumination. Through this analysis, we determined that the local temperature increase is critical to driving the 4-NBT to 4-ABT photoreaction.

EXPERIMENTAL METHODS

Reagents. All chemicals were obtained commercially and used without further purification. Cetyltrimethylammonium bromide (>98.0%), cetyltrimethylammonium chloride (CTAC, 25% water solution), sodium oleate (NaOL, technical grade >82% fatty acid), L-ascorbic acid (AA, >99.9%), 4-NBT, hydrochloric acid (HCl, 37 wt % in water), ethyleneglycol (EG, (99%), poly(vinyl pyrrolidone) (PVP, M_w = 55 000), and sodium sulfide nonahydrate ($Na_2S{\cdot}9H_2O$, analytical grade) were purchased from Sigma-Aldrich. Hydrogen tetrachloroaurate trihydrate ($HAuCl_4{\cdot}3H_2O$) and silver nitrate ($AgNO_3$, >99%) were purchased from Alfa Aesar. Ultrapure water obtained from a Milli-Q Integral 5 system was used in all experiments.

Fabrication of Ag Nanocubes and Au Nanocages. NPs were prepared by a protocol previously reported by Skrabalak et al.,[30] with a minor modification.[31] In the first step, Ag nanocube templates were prepared by mixing 30 mL of EG, a sodium sulfide solution in EG (0.35 mL, 3 mM), a PVP solution in EG (7.5 mL, 20 g/L), and a silver nitrate solution in EG (2.5 mL, 48 g/L) under argon flow at a temperature of 150 °C. The resultant Ag nanocubes were washed by centrifugation (12 000*g*, 30 min) and redispersed in 40 mL of ethanol. The isolated Ag nanocubes were converted into Au nanocages via the galvanic replacement reaction.[31] To this end, 2 mL of the as-prepared nanocube suspension was added to the PVP water solution (100 mL, 1 g/L). The mixture was heated at 100 °C under magnetic stirring, followed by the dropwise addition of 10 mL of 1 mM $HAuCl_4$. The resulting nanocages were washed by centrifugation (12 000*g*, 20 min) and were redispersed in 4 mL of water.

Synthesis of Au@Ag Nanocuboids. First, Au nanorods were prepared by a seed-mediated growth in a binary surfactant mixture as described elsewhere.[32,33] Then, 100 μL of 100 mM $AgNO_3$ solution was added to a mixture of 4 mL of Au nanorods and 12 mL of 20 mM CTAC, followed by the addition of 400 μL of 100 mM ascorbic acid as a reductant.[34] The mixture was incubated and unstirred at 70 °C for 3 h. After that, the obtained Au@Ag nanocuboids were washed and finally redispersed in 4 mL of water.

NP Characterization. Extinction spectra were measured with a SPECORD 250 spectrophotometer (Analytik, Jena, Germany). Transmission electron microscope (TEM) images were obtained with a Libra-120 TEM (Carl Zeiss, Jena, Germany) at the "Simbioz" Center for the Collective Use at IBPPM RAS.

Raman Spectroscopy. Micro-Raman spectroscopy experiments were performed within the spectral range 1000−1700 cm^{-1} using the 532 (green), 638 (red), and 785 (IR) nm lines of solid-state lasers in a XploRA Raman spectrometer. A LabRAM HR800 system was used for the temperature-dependent SERS measurements under green and red laser illumination, 514.7 and 633 nm, respectively. Both spectrometers were coupled to an optical microscope Olympus BX-40. A

DOI: 10.1021/acs.jpcc.7b12101
J. Phys. Chem. C 2018, 122, 5657−5663

100× objective (N.A. 0.9) was used to illuminate the sample and to collect the Raman signal in the backscattering geometry. A long working distance objective was used (50× LWD, N.A. 0.5) for the temperature-dependent experiments. The experiments at different focus distances (power density) were realized using a piezoelectric scanner that varied the laser focus (with a 100 LWD objective, N.A. = 0.7) below and above the sample plane. A charge-coupled device was used for the detection of the Raman signal using a diffraction grating of 600 lines per millimeter, a spectral resolution of at least 4 cm^{-1}, and an acquisition time of 1 s. The laser power was limited to the range 0.5−2 mW to avoid unintended modifications of the molecular layers.

The colloids of Au and Ag NPs were first dropcasted on a Si surface and dried in air. 4-NBT molecules were dissolved in ethanol and used as a stock solution for the functionalization of the metal NPs deposited on Si wafers. The NP-coated silicon wafer was immersed in the 4-NBT solution overnight to ensure the formation of a monolayer of 4-NBT on the surface of NPs. Afterward, the sample was taken out, rinsed gently with ethanol to remove possible physically absorbed molecules, and finally dried under N_2 flow.

Finite-Difference Time-Domain Simulation. Electromagnetic simulations were performed by employing a finite-difference time-domain (FDTD) method using the program of FDTD Solutions (version 8.0, from Lumerical Solutions, Inc.). TEM data were used to obtain geometrical models of the NPs. The simulation volume was a 100 × 100 × 100 nm cube with a uniform mesh of 0.5 nm. In all simulations, the "total scattering field" mode was used together with the Au optical constants taken from the Drude approximation of the Johnson and Christy data.[35] The FDTD "field monitors" were placed in the middle sections of the NPs. The processor time of one simulation run was about 1 h (8 × 2.7 GHz processors, 64 GB RAM).

RESULTS AND DISCUSSION

Figure 1A−C shows the TEM images of NPs used as a catalyst for the photoreduction of NBT. According to these data, the cubes have an average edge length of 50 ± 8 nm and show rounded corners with a diameter of about 5 nm. The TEM images also revealed the presence of particles of triangular shape (not more than 5% of the total amount). In close agreement with the previously reported data,[36] the nanocubes have four overlapping resonance bands between 320 and 550 nm (Figure 1D, curve 1), where the strongest peak at 455 nm is assigned to the dipole plasmon resonance, whereas other peaks are attributed to higher-order plasmon modes.

The TEM image of Au@Ag nanocuboids is shown in Figure 1B. It is clear that these NPs have a cuboidal shape and narrow size and width distributions. The statistical analysis gives the average value of the cuboidal length of 87 ± 6 nm and the width of 44 ± 3 nm. The gold nanorod cores are visible in semitransparent layers consistent with the previous observations.[37,38] It is important to notice that as reported in a previous work, the optical and chemical properties of cuboids are determined by the Ag shell, whereas the influence from the Au nanorod core is minimal.[39] The spectrum of the Au@Ag cuboids (Figure 1D, curve 2) consistently displays plasmon resonance bands associated with a longitudinal mode that appears as a shoulder at 623 nm and three higher-order hybrid modes at 418, 384, and 348 nm.

Previously, we showed that these modes are associated with the cubic transversal cross-section of the Ag cuboid.[39] Figure 1C shows the TEM image of nanocages made by using 50 nm silver cubes as templates. It can be seen that the Au nanocages mostly maintained a cubic shape with an edge length of (53 ± 15) nm and shallow walls. The main LSPR peak for nanocages with such geometrical dimensions is located near 800 nm. The TEM images also revealed the presence of porous particles of triangular shape (not more than 5% of the total amount). The LSPR overlap motivated the choice of our set of NPs as a platform for photoreduction with the laser wavelengths available for the SERS experiments. As a result, the NP hotspots can be excited efficiently under the corresponding light irradiation. For example, Figure 1E shows the results of FDTD simulations of the EM field distribution near the Ag cubes (top), Au@Ag cuboids (middle), and Au nanocages (bottom) under irradiation with 532 nm (left), 638 nm (center), and 785 nm (right). It is clear that Ag nanocubes have a higher field enhancement factor under green laser irradiation, whereas the Au nanocages work better in the NIR region. For Au@Ag cuboids, the wavelength with higher field enhancement depends on the NP orientation with respect to the polarization of incident light. For the longitudinal direction (as shown in Figure 1E), the hotspots occur under red light irradiation, but in the transversal direction, the optical properties of cuboids become very close to those of Ag cubes (data not shown).

Figure 2A,B shows the Raman spectra of 4-ABT (A) and 4-NBT (B) used as a reference in the further study. The most

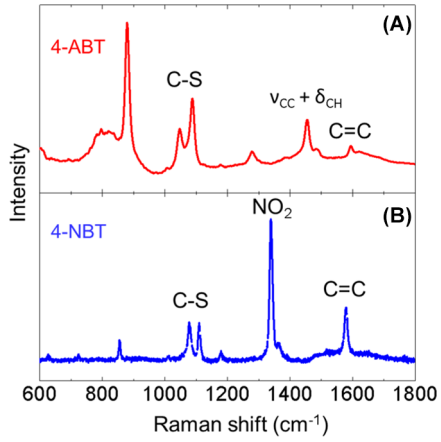

Figure 2. Raman spectra of 4-ABT (A) and 4-NBT (B) measured on a Si wafer under 633 nm laser excitation.

intense SERS peak of 4-NBT located at 1346 cm^{-1} can be assigned to the symmetric stretching vibration of the nitro group $\nu(NO_2)$.[40] The other distinct peaks in Figure 2B can be attributed to the CC ring stretching (1589 cm^{-1}) and C−S vibration (1078 and 1034 cm^{-1}).[41] In the Raman spectra of 4-ABT (Figure 2A), the band at 1443 cm^{-1} originates from the $\nu_{CC} + \delta_{CH}$ ring vibration, whereas the intense band of the nitro group vibration is absent. Thus, the intensity decreases at 1346 cm^{-1} together with the intensity increase of the $\nu_{CC} + \delta_{CH}$ ring vibration at 1443 cm^{-1} are indicative of the photocatalytic transformation of 4-NBT to 4-ABT.[24] This allows us to use the intensity ratio between these two bands as a figure of merit for the photocatalytic reduction of 4-NBT on the different Ag and Au NP systems investigated by SERS. The observation of 4-ABT in SERS was the subject of debate, particularly because of

DOI: 10.1021/acs.jpcc.7b12101
J. Phys. Chem. C 2018, 122, 5657−5663

the close spectral features that 4-ABT has with other azo compounds. Recent reports aimed at clarifying this issue have established that 4-ABT is the sole product of the plasmon-induced photocatalytic reaction of 4-NBT.[29,42]

Figure 3A–C shows the surface-enhanced Raman scattering spectra of 4-NBT adsorbed on Au/Ag nanocages, Ag cubes, and

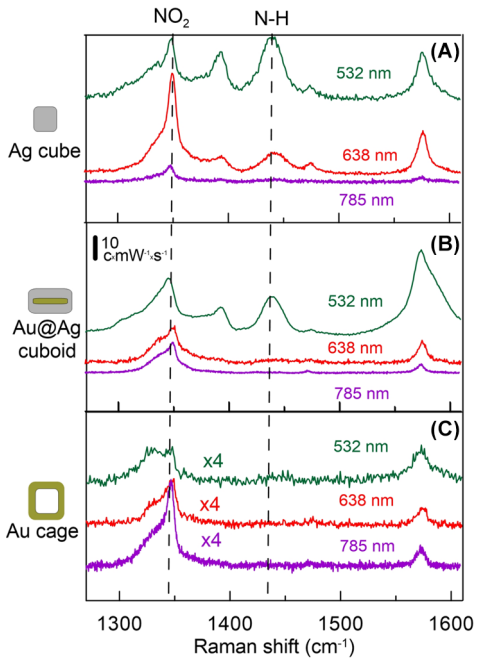

Figure 3. SERS spectra of 4-NBT measured under different laser wavelengths using Ag cubes (A), Au@Ag nanorods (B), and Au nanocages (C). The NH_2 label refers to the $\nu_{CC} + \delta_{CH}$ ring vibration characteristic of 4-ABT. To ensure a proper comparison of the spectra from (a) to (c), in all three NP systems, the laser power was kept constant for a fixed excitation wavelength. The laser power used: 9.7 μW@532 nm, 18.4 μW@638 nm, and 65.3 μW@785 nm.

Au/Ag nanorods, respectively. The role of the LSPR in the photocatalytic reaction is evidenced by using different excitation wavelengths. For example, the 532 nm laser excitation wavelength is close to the main LSPR peak of Ag cubes thus producing hotspots at the nanocube corners (see Figure 1E). First, for the Ag nanocubes, we observe the highest SERS response under green laser excitation. The intensity of Raman lines gradually decreases when shifting to red and NIR light. More importantly, under green and red laser excitation, the band at 1443 cm^{-1} from the $\nu_{CC} + \delta_{CH}$ ring vibration becomes clearly visible. This is a clear indication that the green and red lasers can trigger the photocatalytic reaction of 4-NBT to 4-ABT. Additionally, for Ag nanocubes, the peak intensity at 1443 cm^{-1} is much higher under LSPR condition (under green laser excitation). Surprisingly, the results obtained when using Au@Ag cuboids show SERS spectra quite close to those obtained for Ag cubes. Again, we observe the appearance of the $\nu_{CC} + \delta_{CH}$ mode under green laser irradiation. The main difference is the absence of the distinct photocatalytic reaction in LSPR conditions under red light irradiation. In the case of Au nanocages, as shown in Figure 3C, all the peaks can be attributed to 4-NBT by comparing to the spectra in Figure 2B. Thus, these results show that no photocatalytic activity was detected for the Au nanocages under any of the laser excitations, even when the LSPR was excited at the NIR range. These observations suggest that the plasmon resonance excitation is not sufficient to induce the photoconversion reaction but that other additional mechanism must be involved.

The other important parameter involved in the reaction is the local heating of 4-NBT molecules by the NPs under laser irradiation. This hypothesis is verified in the following. To verify our hypothesis about the temperature-induced mechanism, the Au nanocages were heated up to 150 °C with a temperature ramp rate of 10 °C·min^{-1} and the SERS spectra were recorded under 633 nm laser irradiation (Figure 4A). We focus on the Au nanocages because they do not induce any reaction at room temperature as discussed above. It is clearly seen that during the first four measurements, that is, up to 55 °C, the SERS spectra remain almost unchanged, whereas further increase in the temperature leads to the spectral changes indicative of the 4-NBT to 4-ATP conversion. Figure 4B shows the temperature dependence of the intensity ratio between peaks at 1346 and 1443 cm^{-1}. Below 70 °C, the intensity ratio was between 6.5 and 7.5 and kept almost constant. When the temperature reached 70 °C, a sharp decrease of the intensity ratio between NO_2 vibration and $\nu_{CC} + \delta_{CH}$ ring vibration peaks was observed. The final intensity ratio was below 2. This is a key result that provides further evidence on the influence of local temperature in the photocatalytic reaction.

To determine whether heating the 4-NBT molecules is sufficient to induce their conversion to 4-ABT without a metal catalyst, a Si wafer coated with 4-NBT was investigated under the same temperature program as the Au nanocages. Figure 4C shows the Raman spectra of the Si wafer at 25 and 150 °C. The Raman spectra remain unchanged after heating. For temperatures above 150 °C, the 4-NBT molecules completely evaporated from the substrate without showing the Raman fingerprint peak at 1443 cm^{-1}. Thus, temperatures up to 150 °C for the Si substrate are not sufficient to produce 4-ABT. For this reaction to take place, the molecules need to be in contact with a metal catalyst as was the case for the Au nanocages. Therefore, we investigated further the effect of the chemical contribution by employing a flat Ag substrate that has no LSPR (Figure 4D). To this end, a 4-NBT monolayer on the flat silver surface was obtained under the same conditions as on the NPs. At low laser power, just a small feature representing 4-ABT was observed. When the red laser excitation reached a power of about 1 mW, we observed an intensity increase of the 4-ABT band at 1443 cm^{-1}. After the temperature was increased and reached 150 °C, the intensity of the $\nu_{CC} + \delta_{CH}$ ring vibration became comparable to that of one of the vibrations of the nitro group. This result provides additional evidence that the presence (and excitation) of LSPR is not the only condition for the photocatalytic conversion. Instead, a catalytic surface such as Ag and a threshold temperature are the two essential parameters that trigger the photochemical reaction.

The last piece of evidence of the heating contribution to the 4-NBT to 4-ABT transformation was provided by investigating the Raman spectra evolution on 4-NBT-coated Au@Ag cuboids as a function of power density under 638 nm irradiation. The results are shown in Figure 5A. A controlled change in power density at the same spot of the sample was achieved by the linear motion of a high N.A. (0.9) objective in the Raman microscope in the direction normal to the sample surface. The objective was moved from a focal point above the sample plane to a position below, inside the sample, obtaining the Raman spectra shown in the two-dimensional (2D) plot in Figure 5A. Figure 5A shows the evolution of the power density

DOI: 10.1021/acs.jpcc.7b12101
J. Phys. Chem. C 2018, 122, 5657–5663

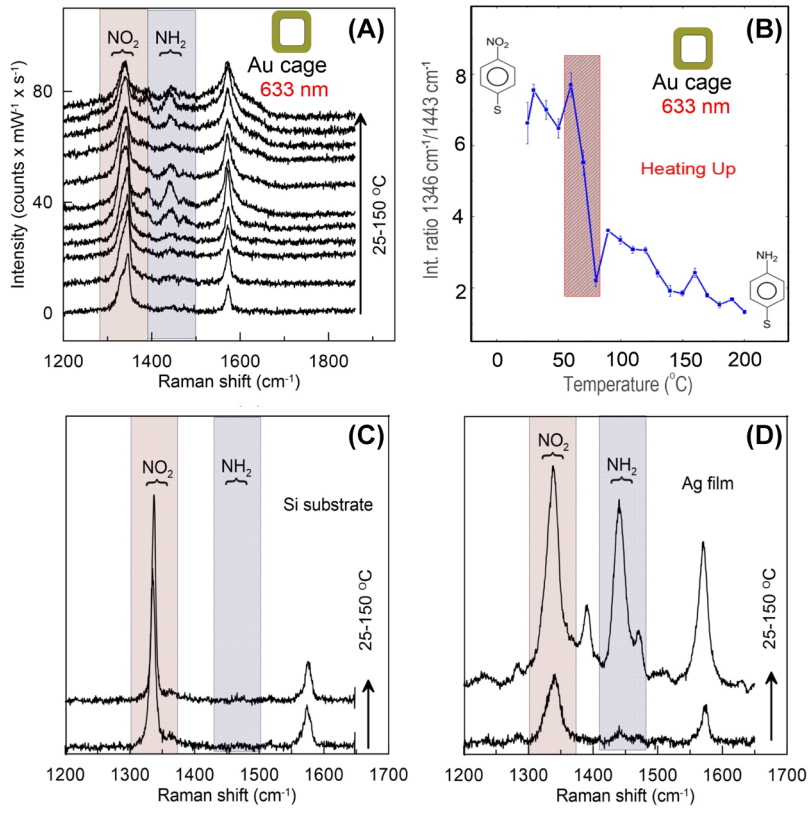

Figure 4. (A) SERS spectra of 4-NBT adsorbed on Au nanocages measured under 633 nm laser excitation with the temperature varied from 25 to 150 °C. (B) Dependence of the intensity ratio between peaks at 1346 and 1443 cm^{-1} vs temperature. Raman spectra of 4-NBT on the Si substrate (C) and the flat Ag surface (D) before and after heating to 150 °C under 633 nm laser excitation. The NH_2 label refers to the $\nu_{CC} + \delta_{CH}$ ring vibration characteristic of 4-ABT.

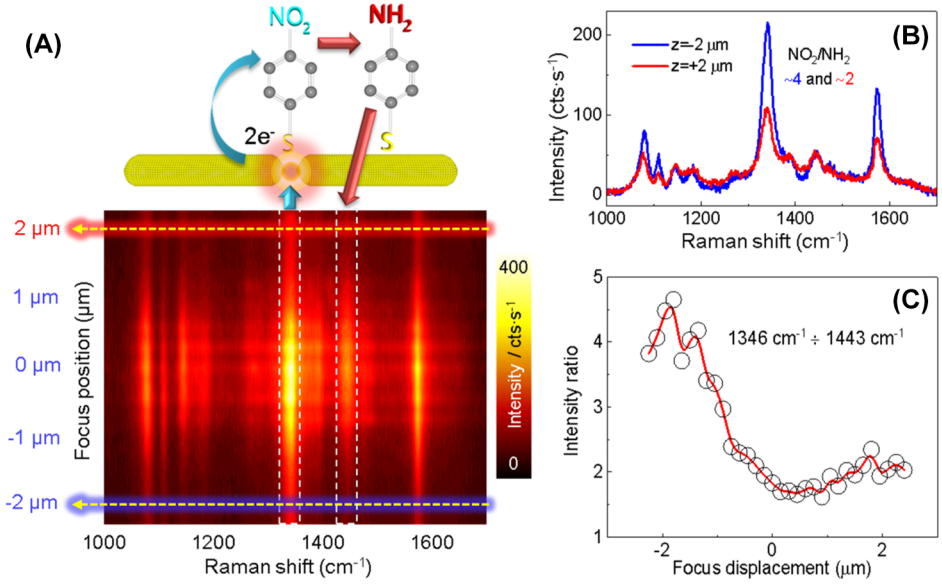

Figure 5. (A) Sketch of the hot electron transfer during the NBT to ABT transformation on the Au@Ag cuboid substrate under 638 nm laser excitation. The two main Raman modes from these two species are marked in the 2D spectra graph below. Raman spectra evolution as a function of focus displacement (power density). (B) Raman spectra before (blue) and after (red) focusing. (C) Intensity ratio (1346 cm^{-1}/1443 cm^{-1}) decreases by a factor of 2 after focusing. The NH_2 label refers to the $\nu_{CC} + \delta_{CH}$ ring vibration characteristic of 4-ABT.

represented by the intensity profile of the most intense Raman mode at 1346 cm^{-1}. The spectra shown in Figure 5B were obtained at the focus positions −2 and +2 μm corresponding to the cases before and after reaching the max power density (at 0 μm), respectively. Increasing the power density leads to an increase in the local temperature which in turn induced the irreversible transformation of 4-NBT to 4-ABT. This observation is confirmed by the decrease in the intensity ratio between the Raman modes of both components, as illustrated in Figure 5C. Importantly, the SERS intensity ratio between the

DOI: 10.1021/acs.jpcc.7b12101
J. Phys. Chem. C 2018, 122, 5657−5663

peaks due to the vibration of the nitro group and the stretching vibration of N−H decreases during focusing, but it does not increase after defocusing. This result further confirms that the transformation of 4-NBT to 4-ABT depends on the local temperature of hotspots which is here dependent on the laser power density. As shown by the FDTD simulation results in Figure 1E, the electric field and therefore the power density become extremely high at the NP hotspots. The results in Figure 5B show that high power density triggers the photocatalytic reaction from 4-NBT to 4-ABT (as illustrated by the change in the intensity ratio). Notice that on contrary to the Raman spectrum shown in Figure 3B, the spectrum in Figure 5B already shows the mode from 4-ABT at 1443 cm^{-1}. Because both spectra were obtained using the same laser energy and the same NP system, this apparent inconsistency is attributed to the differences in power densities. The N.A. of the objective (see Experimental Methods) and the laser power were not the same, although being higher for the spectrum in Figure 5B with respect to the spectrum in Figure 3B. A higher laser power was required for the results in Figure 5A because only nonzero values of the 4-ABT band allowed a proper estimation of the changes in the intensity ratio reported in Figure 5C.

This systematic study involving different metallic NPs with resonances spanning a broad spectral range, the multiwavelength, and the temperature-dependent SERS investigation including nonplasmonic surfaces allows us to revisit the widely accepted idea that the excitation of hot electrons and not the temperature is the deciding factor in plasmon-induced catalytic reactions.[43] For example, in ref 22, it was stated that one only needs hot electrons excited at active sites of Ag NPs to induce the photocatalytic conversion of 4-NBT to 4-ABT.[22] Even more recently, the same group reported a cryogenic SERS study in ref 29 explicitly ruling out the role of temperature.[29] Moreover, in the plasmon-induced photocatalytic oxidation of pollutants, it was concluded that not only the hot electrons excitation and charge transfer were the factors responsible for the reaction but also the energy accumulation in the vibrational mode of O_2 plays a role in lowering the dissociation energy.[44] We expand this idea further and demonstrated in this work that in contrast to the general belief, the localized temperature is a critical driving force for the plasmon-induced photocatalytic reaction and not only the excitation of hot electrons.[43]

CONCLUSIONS

The substrate-, wavelength-, and temperature-dependent surface catalysis reaction from 4-NBT to 4-ABT by surface plasmon resonances on Au, Ag, and composite NPs were systematically investigated. Using this molecular model system self-assembled on different kinds of plasmonic NPs, we showed that local heating is a key to drive the plasmon-induced chemical reaction of 4-NBT to 4-ABT. It is worth noticing that the increase of the localized temperature at hotspots made by plasmonic NPs is expected to be always present in the plasmon-induced reactions. This universality is due to the excitation of conduction electrons by the electric field of light-inducing collisions with the ion lattice of the plasmonic NPs. These electron-ion scattering events translate into heat generation. This itself makes the localized thermal contribution a general and critical point that we should always consider, and this observation is precisely what our experimental results and analyses demonstrate. Ongoing and future engineering of plasmonics in fields such as water splitting, chemical synthesis, and energy harvesting can now exploit the role of localized temperature to maximize the conversion efficiency that defines the fate of these emerging nanotechnologies.

AUTHOR INFORMATION

Corresponding Author

*E-mail: raulmet@gmail.com.

ORCID

Raul D. Rodriguez: 0000-0003-4016-1469

Notes

The authors declare no competing financial interest.

ACKNOWLEDGMENTS

A.A.G. thanks InProTUC program for funding this research. The work of B.N.K. was supported by RFBR grants (nos. 17-02-00075 and 16-02-00054). This work was supported by the DFG Research Unit FOR1713 SMINT and the Cluster of Excellence "Center for Advancing Electronics Dresden" (cfaed). The research was partly funded by Tomsk Polytechnic University Competitiveness Enhancement Program grant, project number TPU CEP_IHTP_73\2017. This work was performed in the context of the EU COST Action MP1302 Nanospectroscopy.

REFERENCES

(1) van Schrojenstein Lantman, E. M.; Deckert-Gaudig, T.; Mank, A. J. G.; Deckert, V.; Weckhuysen, B. M. Catalytic Processes Monitored at the Nanoscale with Tip-Enhanced Raman Spectroscopy. *Nat. Nanotechnol.* **2012**, *7*, 583−586.

(2) Okawa, Y.; Aono, M. Materials Science: Nanoscale Control of Chain Polymerization. *Nature* **2001**, *409*, 683−684.

(3) Cordeiro, D. S.; Corio, P. Electrochemical and Photocatalytic Reactions of Polycyclic Aromatic Hydrocarbons Investigated by Raman Spectroscopy. *J. Braz. Chem. Soc.* **2009**, *20*, 80−87.

(4) Han, H. S.; Han, S. W.; Kim, C. H.; Kim, K. Adsorption and Reaction of 4-Nitrobenzoic Acid on Ω-Functionalized Alkanethiol Monolayers on Powdered Silver: Infrared and Raman Spectroscopy Study. *Langmuir* **2000**, *16*, 1149−1157.

(5) Han, S. W.; Lee, I.; Kim, K. Patterning of Organic Monolayers on Silver Via Surface-Induced Photoreaction. *Langmuir* **2002**, *18*, 182−187.

(6) Christopher, P.; Xin, H.; Marimuthu, A.; Linic, S. Singular Characteristics and Unique Chemical Bond Activation Mechanisms of Photocatalytic Reactions on Plasmonic Nanostructures. *Nat. Mater.* **2012**, *11*, 1044−1050.

(7) Kneipp, K.; Wang, Y.; Kneipp, H.; Perelman, L. T.; Itzkan, I.; Dasari, R. R.; Feld, M. S. Single Molecule Detection Using Surface-Enhanced Raman Scattering (SERS). *Phys. Rev. Lett.* **1997**, *78*, 1667.

(8) Duan, S.; Ai, Y.-J.; Hu, W.; Luo, Y. Roles of Plasmonic Excitation and Protonation on Photoreactions of P-Aminobenzenethiol on Ag Nanoparticles. *J. Phys. Chem. C* **2014**, *118*, 6893−6902.

(9) Ueno, K.; Misawa, H. Surface Plasmon-Enhanced Photochemical Reactions. *J. Photochem. Photobiol., C* **2013**, *15*, 31−52.

(10) Kafle, B.; Poveda, M.; Habteyes, T. G. Surface Ligand-Mediated Plasmon-Driven Photochemical Reactions. *J. Phys. Chem. Lett.* **2017**, *8*, 890−894.

(11) Kale, M. J.; Avanesian, T.; Christopher, P. Direct Photocatalysis by Plasmonic Nanostructures. *ACS Catal.* **2014**, *4*, 116−128.

(12) Silva, C. G.; Juárez, R.; Marino, T.; Molinari, R.; García, H. Influence of Excitation Wavelength (Uv or Visible Light) on the Photocatalytic Activity of Titania Containing Gold Nanoparticles for the Generation of Hydrogen or Oxygen from Water. *J. Am. Chem. Soc.* **2011**, *133*, 595−602.

(13) Ingram, D. B.; Linic, S. Water Splitting on Composite Plasmonic-Metal/Semiconductor Photoelectrodes: Evidence for Selective Plasmon-Induced Formation of Charge Carriers near the Semiconductor Surface. *J. Am. Chem. Soc.* **2011**, *133*, 5202−5205.

DOI: 10.1021/acs.jpcc.7b12101
J. Phys. Chem. C 2018, 122, 5657−5663

(14) Seh, Z. W.; Liu, S.; Low, M.; Zhang, S.-Y.; Liu, Z.; Mlayah, A.; Han, M.-Y. Janus Au-Tio2 Photocatalysts with Strong Localization of Plasmonic near-Fields for Efficient Visible-Light Hydrogen Generation. *Adv. Mater.* **2012**, *24*, 2310−2314.
(15) Mukherjee, S.; Libisch, F.; Large, N.; Neumann, O.; Brown, L. V.; Cheng, J.; Lassiter, J. B.; Carter, E. A.; Nordlander, P.; Halas, N. J. Hot Electrons Do the Impossible: Plasmon-Induced Dissociation of H2 on Au. *Nano Lett.* **2013**, *13*, 240−247.
(16) Lee, Y. K.; Jung, C. H.; Park, J.; Seo, H.; Somorjai, G. A.; Park, J. Y. Surface Plasmon-Driven Hot Electron Flow Probed with Metal-Semiconductor Nanodiodes. *Nano Lett.* **2011**, *11*, 4251−4255.
(17) Hou, W.; Hung, W. H.; Pavaskar, P.; Goeppert, A.; Aykol, M.; Cronin, S. B. Photocatalytic Conversion of Co2 to Hydrocarbon Fuels Via Plasmon-Enhanced Absorption and Metallic Interband Transitions. *ACS Catal.* **2011**, *1*, 929−936.
(18) Kim, K.; Choi, J.-Y.; Shin, K. S. Photoreduction of 4-Nitrobenzenethiol on Au by Hot Electrons Plasmonically Generated from Ag Nanoparticles: Gap-Mode Surface-Enhanced Raman Scattering Observation. *J. Phys. Chem. C* **2015**, *119*, 5187−5194.
(19) Kim, K.; Lee, I.; Lee, S. J. Photolytic Reduction of 4-Nitrobenzenethiol on Au Mediated Via Ag Nanoparticles. *Chem. Phys. Lett.* **2003**, *377*, 201−204.
(20) Ren, X.; Tan, E.; Lang, X.; You, T.; Jiang, L.; Zhang, H.; Yin, P.; Guo, L. Observing Reduction of 4-Nitrobenzenthiol on Gold Nanoparticles in Situ Using Surface-Enhanced Raman Spectroscopy. *Phys. Chem. Chem. Phys.* **2013**, *15*, 14196−14201.
(21) Shin, K. S.; Lee, H. S.; Joo, S. W.; Kim, K. Surface-Induced Photoreduction of 4-Nitrobenzenethiol on Cu Revealed by Surface-Enhanced Raman Scattering Spectroscopy. *J. Phys. Chem. C* **2007**, *111*, 15223−15227.
(22) Lee, S. J.; Kim, K. Surface-Induced Photoreaction of 4-Nitrobenzenethiol on Silver: Influence of Sers-Active Sites. *Chem. Phys. Lett.* **2003**, *378*, 122−127.
(23) Dong, B.; Fang, Y.; Chen, X.; Xu, H.; Sun, M. Substrate-, Wavelength-, and Time-Dependent Plasmon-Assisted Surface Catalysis Reaction of 4-Nitrobenzenethiol Dimerizing to P, P′-Dimercaptoazobenzene on Au, Ag, and Cu Films. *Langmuir* **2011**, *27*, 10677−10682.
(24) Shin, K. S.; Cho, Y. K.; Kim, K. Surface-Enhanced Raman Scattering Characteristics of 4-Nitrobenzenethiol Adsorbed on Palladium and Silver Thin Films. *Vib. Spectrosc.* **2014**, *70*, 120−124.
(25) Kim, M.; Lin, M.; Son, J.; Xu, H.; Nam, J.-M. Hot-Electron-Mediated Photochemical Reactions: Principles, Recent Advances, and Challenges. *Adv. Opt. Mater.* **2017**, *5*, 1700004.
(26) Chadha, R.; Maiti, N.; Kapoor, S. Catalytic Reactions on the Surface of Ag Nanoparticles: A Photochemical Effect and/or Molecule Property? *J. Phys. Chem. C* **2014**, *118*, 26227−26235.
(27) Zhao, L.-B.; Zhang, M.; Huang, Y.-F.; Williams, C. T.; Wu, D.-Y.; Ren, B.; Tian, Z.-Q. Theoretical Study of Plasmon-Enhanced Surface Catalytic Coupling Reactions of Aromatic Amines and Nitro Compounds. *J. Phys. Chem. Lett.* **2014**, *5*, 1259−1266.
(28) Huang, Y.-F.; Wu, D.-Y.; Zhu, H.-P.; Zhao, L.-B.; Liu, G.-K.; Ren, B.; Tian, Z.-Q. Surface-Enhanced Raman Spectroscopic Study of P-Aminothiophenol. *Phys. Chem. Chem. Phys.* **2012**, *14*, 8485−8497.
(29) Kim, K.; Choi, J.-Y.; Shin, K. S. Surface-Enhanced Raman Scattering of 4-Nitrobenzenethiol and 4-Aminobenzenethiol on Silver in Icy Environments at Liquid Nitrogen Temperature. *J. Phys. Chem. C* **2014**, *118*, 11397−11403.
(30) Skrabalak, S. E.; Au, L.; Li, X.; Xia, Y. Facile Synthesis of Ag Nanocubes and Au Nanocages. *Nat. Protoc.* **2007**, *2*, 2182−2190.
(31) Khlebtsov, B.; Panfilova, E.; Khanadeev, V.; Bibikova, O.; Terentyuk, G.; Ivanov, A.; Rumyantseva, V.; Shilov, I.; Ryabova, A.; Loshchenov, V. Nanocomposites Containing Silica-Coated Gold−Silver Nanocages and Yb−2, 4-Dimethoxyhematoporphyrin: Multifunctional Capability of Ir-Luminescence Detection, Photosensitization, and Photothermolysis. *ACS Nano* **2011**, *5*, 7077−7089.
(32) Ye, X.; Zheng, C.; Chen, J.; Gao, Y.; Murray, C. B. Using Binary Surfactant Mixtures to Simultaneously Improve the Dimensional Tunability and Monodispersity in the Seeded Growth of Gold Nanorods. *Nano Lett.* **2013**, *13*, 765−771.
(33) Khlebtsov, B. N.; Khanadeev, V. A.; Ye, J.; Sukhorukov, G. B.; Khlebtsov, N. G. Overgrowth of Gold Nanorods by Using a Binary Surfactant Mixture. *Langmuir* **2014**, *30*, 1696−1703.
(34) Khlebtsov, B.; Khanadeev, V.; Khlebtsov, N. Surface-Enhanced Raman Scattering inside Au@Ag Core/Shell Nanorods. *Nano Res.* **2016**, *9*, 2303−2318.
(35) Johnson, P. B.; Christy, R. W. Optical Constants of the Noble Metals. *Phys. Rev. B: Solid State* **1972**, *6*, 4370.
(36) Panfilova, E. V.; Khlebtsov, B. N.; Burov, A. M.; Khlebtsov, N. G. Study of Polyol Synthesis Reaction Parameters Controlling High Yield of Silver Nanocubes. *Colloid J.* **2012**, *74*, 99−109.
(37) Xiang, Y.; Wu, X.; Liu, D.; Li, Z.; Chu, W.; Feng, L.; Zhang, K.; Zhou, W.; Xie, S. Gold Nanorod-Seeded Growth of Silver Nanostructures: From Homogeneous Coating to Anisotropic Coating. *Langmuir* **2008**, *24*, 3465−3470.
(38) Ah, C. S.; Hong, S. D.; Jang, D.-J. Preparation of Aucoreagshell Nanorods and Characterization of Their Surface Plasmon Resonances. *J. Phys. Chem. B* **2001**, *105*, 7871−7873.
(39) Khlebtsov, B. N.; Liu, Z.; Ye, J.; Khlebtsov, N. G. Au@Ag Core/Shell Cuboids and Dumbbells: Optical Properties and Sers Response. *J. Quant. Spectrosc. Radiat. Transfer* **2015**, *167*, 64−75.
(40) Skadtchenko, B. O.; Aroca, R. Surface-Enhanced Raman Scattering of P-Nitrothiophenol Molecular Vibrations of Its Silver Salt and the Surface Complex Formed on Silver Islands and Colloids. *Spectrochim. Acta, Part A* **2001**, *57*, 1009−1016.
(41) Ye, J.; Hutchison, J. A.; Uji-i, H.; Hofkens, J.; Lagae, L.; Maes, G.; Borghs, G.; Van Dorpe, P. Excitation Wavelength Dependent Surface Enhanced Raman Scattering of 4-Aminothiophenol on Gold Nanorings. *Nanoscale* **2012**, *4*, 1606−1611.
(42) Kim, K.; Yoon, J. K.; Lee, H. B.; Shin, D.; Shin, K. S. Surface-Enhanced Raman Scattering of 4-Aminobenzenethiol in Ag Sol: Relative Intensity of A1- and B2-Type Bands Invariant against Aggregation of Ag Nanoparticles. *Langmuir* **2011**, *27*, 4526−4531.
(43) Zhang, Y.; He, S.; Guo, W.; Hu, Y.; Huang, J.; Mulcahy, J. R.; Wei, W. D. Surface-Plasmon-Driven Hot Electron Photochemistry-*Chem. Rev.* 2017.
(44) Christopher, P.; Xin, H.; Linic, S. Visible-Light-Enhanced Catalytic Oxidation Reactions on Plasmonic Silver Nanostructures. *Nat. Chem.* **2011**, *3*, 467−472.

DOI: 10.1021/acs.jpcc.7b12101
J. Phys. Chem. C 2018, 122, 5657−5663